Measurement of Thermal Lensing in Cr^{3+}-Doped Colquiriites

Jason M. Eichenholz and Martin Richardson

***Abstract*— The first direct measurements of thermally induced lensing in end-pumped Cr^{3+}-doped LiSAF, LiSGAF, LiSCAF, and LiCAF are reported. Using a sensitive measurement technique, focal lengths as long as 40 m were measured. A thermal model has been created to determine the temperature rise as a function of position inside the laser crystal. This new model calculates the temperature distribution by considering quantum defect, upconversion, and upper state lifetime quenching as heating sources. Thermal lensing in the colquiriites is significantly reduced because of compensation of the temperature-dependent refractive index by the induced photoelastic stress inside the colquiriite crystal.**

***Index Terms*— Chromium materials, laser beam distortions, laser measurements, laser thermal factors, solid lasers.**

I. Introduction

LONGITUDINAL diode pumping of a solid-state laser material has the advantage of highly efficient fundamental mode operation [1]. In this form of pumping, the pump power is focused directly into the center of the laser rod and thus is absorbed predominately in the TEM_{00} laser mode volume [2]. Transverse pumping on the other hand tends to distribute the pump power throughout the entire laser rod volume, which leads to multimode operation [1]. As a result of the pump power being concentrated near the center of the crystal, a thermal gradient is produced. The thermal gradient is the result of the strongly inhomogeneous thermal power density that heats the center of the crystal while the edges of the rod remain cool. This heating leads to stress, birefringence, surface elongation, refractive index variation, thermal lensing, and ultimately mechanical fracture [3]. These thermal effects initially hindered the reliable operation and scaling of diode-pumped Nd^{3+} laser systems to increasingly higher average power levels [1], [4]. The measurement and compensation of these induced thermal effects in new solid-state media is therefore crucial to the scaling of new laser systems to higher powers. The development of high-power diode-pumped colquiriite lasers has for a long time been limited by the availability of high-power visible laser diode sources. However, the recent development of 670-nm laser diode arrays [5]–[9] has led to the initial development of compact high-average-power (>1 W) laser sources [10].

Many of the important laser parameters such as small-signal gain [11]–[15], excited stated absorption [16]–[18], and upconversion [16]–[20] have been measured in the colquiriites. In addition, many of the thermomechanical properties such as thermal conductivity [12], [21]–[23], upper state lifetime quenching [24], temperature-dependent refractive index [22], [25], thermal expansion [22], [23], [25], and fracture strength [21]–[23] have also been measured.

Thermal lensing has not yet been considered in end-pumped colquiriite laser systems. It plays one of the key roles in limiting and degrading lasing performance in end-pumped laser systems by producing a lens-like focusing effect inside the laser media [26]. Thermal lensing in a laser system was first reported by Gordon *et al.* [27] in 1964 and an expression for the focal length of the medium was derived. Since then, much work has been done on the analysis of thermal lensing in transverse [22], [28] and end-pumped lasers [3], [29]. If the power of the thermal lens is too large, it is possible that the laser cavity can become unstable and the system will stop lasing [3]. It has also been shown that the separation of the mirrors inside a folded cavity is critical to achieving stable self-starting in Kerr lens mode-locked (KLM) cavities [30]. Recently, the KLM theory has been improved to take account of gain guiding and astigmatism [31]. The magnitude and sign of a thermal lens inside a crystal is important data that could be included in calculations regarding KLM cavity stability. Thermal lensing is one of the major factors that degrades and limits performance in longitudinally pumped solid-state lasers.

In this paper, we describe the measurement and analysis of thermal lensing in Cr^{3+}-doped LiSAF, LiSGAF, LiSCAF, and LiCAF. To the best of our knowledge, this is the first time that thermal lensing of longitudinal pumped Cr^{3+}-doped colquiriites has been measured.

II. Thermal Effects

Many authors [3], [12], [14], [29], [32], [33] have reported on the thermal dynamics of longitudinal diode-pumped solid-state lasers. To understand the thermal dynamics inside the laser rod under longitudinal pumping, a new thermal distribution computer code was constructed. The purpose of this code was to predict the pump-induced temperature rise as a function of radius and length inside the colquiriite laser crystals. The output of this code will be used to help explain the results of the thermal lensing measurements. The model of the thermal effects within the laser rod assumes a CW pump source illuminating the rod from one end, as shown in Fig. 1. The figure shows a side view and an end view of the laser crystal and heat sink geometry assumed in the model. The circumference of the cylindrical laser crystal is

Manuscript received September 16, 1997; revised January 29, 1998.

The authors are with the Center for Research and Education in Optics and Lasers, University of Central Florida, Orlando, FL 32816-2700 USA.

Publisher Item Identifier S 0018-9197(98)03069-3.

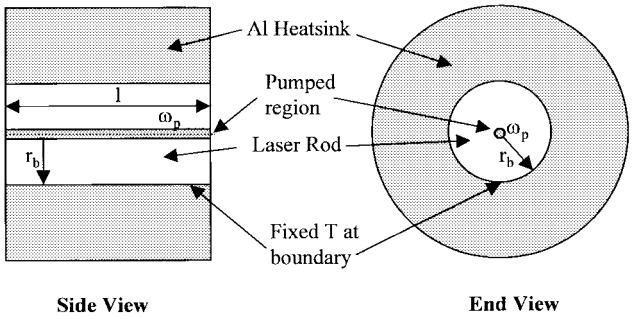

Fig. 1. Side view and end view of an end-pumped colquiriite laser rod. The rod is conductivly cooled by an air-cooled aluminum heat sink. The radius of the rod is r_b, the $1/e^2$ pump spot size of the pump beam is ω_p, and the length of the rod is l.

assumed to be held at a constant temperature by a heat sink surrounding the laser rod. In this geometry, most of the heat is generated inside a small volume near the center of the crystal and is removed from the radial surface via conduction, resulting in a radial temperature gradient inside the rod. This configuration is significantly different from transversely pumped lamp geometries in which a more uniform pumping distribution is achieved [34].

A. Spatial Temperature Distribution

The model determines the three-dimensional (3-D) temperature profile $T(r,z)$ inside the laser rod using the classical heat flow equation [26], [35], [36]

$$-k\cdot\nabla^2 T(r,z)=Q(r,z) \tag{1}$$

where $Q(r,z)$ is the thermal power density (W/cm^3) and k is thermal conductivity (W/K·cm). It assumes that the heat flow is not influenced by axial conduction except near the end faces of the laser rod and that to first order the heat conduction is primarily radial, with negligible longitudinal (z) heat flow. The heat flow equation then becomes purely radial [1], [32]

$$\frac{1}{r}\frac{\partial}{\partial r}\left(r\frac{\partial T(r,z)}{\partial r}\right)+\frac{Q(r,z)}{k}=0. \tag{2}$$

If it is assumed that the heating source $Q(r,z)$ has a Gaussian radial distribution and an exponential decay along the length of the rod, the analytic solution to the differential equation above is given by Innocenzi *et al.* [32] as

$$T(r,z)=T(b)+\frac{\varepsilon P\alpha e^{-\alpha z}}{4\pi K}\cdot\left[\ln\left(\frac{r_b^2}{r^2}\right)+E_1\left(\frac{2r_b^2}{\omega_p^2}\right)-E_1\left(\frac{2r^2}{\omega_p^2}\right)\right] \tag{3}$$

where $T(r,z)$ is the temperature of the rod (K) as a function of radius and length, $T(b)$ is the constant temperature at the surface of the rod, P is the input pump power (W), ε is the percentage of the pump power converted into heat, α is the absorption coefficient of the pump light (cm^{-1}), ω_p is the $1/e^2$ Gaussian radius of the pump beam (cm), and E_1 is the exponential integral function defined as

$$E_1(\chi)=\int_\chi^\infty\frac{e^{-t}}{t}\,dt \tag{4}$$

for $(|\arg\chi|<\pi)$ [37].

B. Heating Sources

To determine the temperature profile inside the laser material, it is necessary to know how much of the pump power is converted into heat. Heating results whenever the energy from a radiative transition (photon) is converted into a nonradiative transition (phonon) inside the crystal. There are three principle mechanisms that give rise to nonradiative transitions in the colquiriites; the quantum defect, upconversion, and thermal quenching of the upper state lifetime. These nonradiative mechanisms can be detrimental heating sources, limiting the amount of output power from a laser system. An assessment of the heating effects of these processes is required in order to estimate the temperature distribution inside the rod.

1) Quantum Defect: Quantum defect heating results from nonradiative transitions inside the crystal lattice due to the difference of the photon energy at the pump wavelength (λ_p) and photon energy at the center wavelength of the laser material's fluorescence (λ_c). As illustrated in the energy level diagrams in Fig. 2, every pump photon absorbed by the crystal and excited into the $^4T_2$ upper laser level deposits a fraction of its energy into the crystal lattice as it nonradiatively relaxes to the bottom of the $^4T_2$ level. After the excited ion radiatively decays to the $^4A_2$ level, additional heat is deposited by the ion as it decays down to the ground state of the laser. To quantify the contribution of quantum defect heating, the pumping rate $R_p(r,z)$ is defined as the number of atoms excited into the upper laser level per second per unit volume [14]

$$R_p(r,z)=\frac{2\lambda_p P_{\rm po}\alpha_p}{hc\pi\omega_p^2(z)}\exp(-\alpha_p z)\exp\left(\frac{-2r^2}{\omega_p^2(z)}\right) \tag{5}$$

where $P_{\rm po}$ is the pump power incident on the crystal (W), α_p is the absorption coefficient at the pump wavelength (cm^{-1}), and n is the refractive index of the crystal. We assume that the pump beam ω_p has a Gaussian spatial distribution

$$\omega_p^2(z)=\omega_{\rm po}^2(z)\left[1+\left(\frac{\lambda_p z}{n\pi\omega_{\rm po}^2}\right)^2\right] \tag{6}$$

where $\omega_{\rm po}$ is the beam waist of the pump laser.

The thermal power density induced by quantum defect heating of a laser crystal is defined as [14]

$$Q_{\rm qd}=\frac{dP_{\rm qd}}{dV}=hc\left(\frac{1}{\lambda_p}-\frac{1}{\lambda_c}\right)R_p \tag{7}$$

where h is Planck's constant. Equation (7) shows that, as the pump wavelength approaches the center fluorescence wavelength, quantum defect heating is reduced.

2) Upconversion: Upconversion occurs in the Cr^{3+} colquiriites when two excited ions in the upper metastable laser level $^4T_2$ interact and exchange energy. As shown in the energy level diagram in Fig. 2, one ion transfers its energy to a neighbor ion, causing it to decay to the $^4A_2$ ground state. The energy transfer promotes the second ion into a higher lying $^4T_1$ excited state. Heating occurs when the excited ions in the $^4T_1$ state nonradiatively decay back down to the upper laser level $^4T_2$. This nonradiative relaxation results in a quantum of the fluorescence energy contributing to heating of the lattice [21]. The rate of upconversion in a laser system is proportional

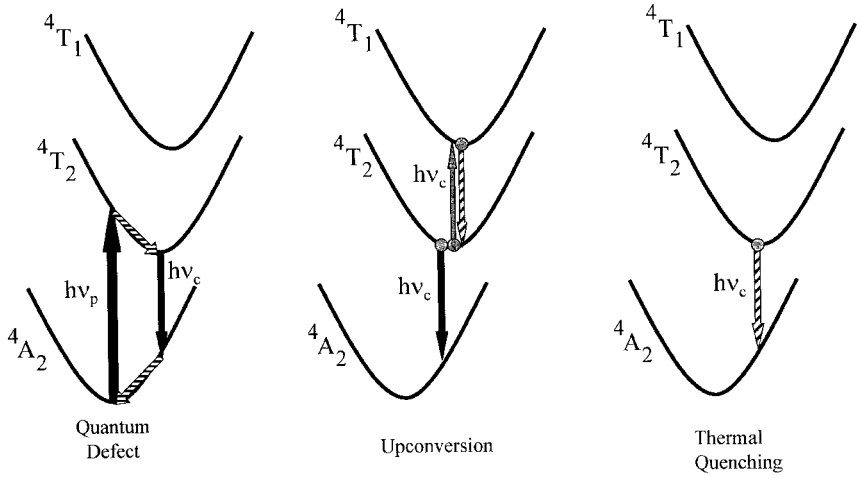

Fig. 2. Energy level diagrams illustrating quantum defect, upconversion, and thermal quenching heating in the Cr^{3+}-doped colquiriites.

to the square of the upper state population density. As the pump power is increased, the upper state population density increases. An increase in population density leads to additional upconversion heating. To quantify the thermal power density contribution from upconversion, the upper state population density must be determined. We begin with the steady-state rate equations for a CW pumping of a quasi-four-level laser system [4]

$$\frac{\partial N_2(r,z)}{\partial t} = R_p(r,z) - \frac{N_2(r,z)}{\tau(r,z)} - ((\sigma - \sigma_{\rm esa})\phi c N_2(r,z)) - (\gamma(N_2(r,z))^2 \tag{8}$$

where $\tau(r,z)$ is the upper state lifetime (s), γ is the upconversion parameter (cm^3/s), σ is the emission cross section (cm^2), $\sigma_{\rm esa}$ is the excited state absorption cross section (cm^2) and ϕ is the laser intensity (W/cm^2) [16], [20]. The terms in (8) describe the pumping rate, spontaneous emission, stimulated emission, excited state absorption, and upconversion, respectively. Solving (8) for the upper state population density while assuming no stimulated emission and excited state absorption gives

$$N_2(r,z) = \frac{\sqrt{1+4\gamma\tau^2(r,z)R_p(r,z)}-1}{2\gamma\tau(r,z)}. \tag{9}$$

The assumptions of no stimulated emission and no excited state absorption are made in this case to compare the predictions of the code with the measurements of the thermal lensing of media that were not in a laser resonator. Once $N_2(r,z)$ is known, the thermal power density for upconversion is given as [14]

$$Q_{\rm up} = \frac{dP_{\rm up}}{dV} = \frac{hc}{\lambda_p}\gamma N_2^2(r,z). \tag{10}$$

3) Thermal Quenching of Fluorescence: The fluorescence lifetime of Cr^{3+} ions in the colquiriite host displays a significant temperature dependence [24]. At low temperatures, the upper state lifetime is nearly constant with respect to temperature. As the temperature of the crystal increases, the lifetime drops rapidly.

We define the critical temperature as the temperature at which the upper state lifetime of the material drops to one-half of the radiative decay lifetime at room temperature (25 °C). This strong lifetime dependence on temperature results from the fact that for each colquiriite there is a temperature above which the normal radiative decay between the $^4T_1$ and $^4A_2$ states gives way to faster nonradiative processes. The upper state lifetime $\tau(r,z)$ of a fluorescent ion at a position (r,z) in a crystal is described as

$$\frac{1}{\tau(r,z)} = \frac{1}{\tau_r} + \frac{1}{\tau_{\rm nr}(r,z)} \tag{11}$$

where

$$\tau_{\rm nr}(r,z) = \tau_{\rm nr}^0 \exp\left(\frac{\Delta E}{kT(r,z)}\right) \tag{12}$$

and where τ_r is the radiative lifetime, $\tau_{\rm nr}$ is the nonradiative lifetime, $\tau_{\rm nr}^0$ is the nonradiative lifetime at low temperatures (77 K), k is the Boltzmann constant, and ΔE is the activation energy [24]. The activation energy is the energy difference between the vibrational ground state energy of the $^4T_2$ level and the energy at which the $^4T_2$ and $^4A_2$ potential energy surfaces cross. Table I lists these constants for several colquiriites. The upper state lifetime $\tau_r(r,z)$ can be determined by solving (11)

$$\tau(r,z) = \frac{\tau_r\tau_{\rm nr}(r,z)}{\tau_r + \tau_{\rm nr}(r,z)}. \tag{13}$$

The thermal quenching of fluorescence thermal power density is given as [14]

$$Q_{\rm tq} = \frac{dP_{\rm tq}}{dV} = \frac{hcN_2(r,z)}{\lambda_p\tau_{\rm nr}(r,z)}. \tag{14}$$

4) Total Thermal Power Density: With the thermal power density for each individual heating source known, the total thermal power density is determined by summing the contributions of each heating source. The total thermal power density is given as

$$\frac{dP_{\rm th}(r,z)}{dV} = \frac{dP_{\rm qd}(r,z)}{dV} + \frac{dP_{\rm up}(r,z)}{dV} + \frac{dP_{\rm tq}(r,z)}{dV}. \tag{15}$$

TABLE I
PHYSICAL AND OPTICAL PARAMETERS OF COLQUIRIITES

Parameter	LiSAF	LiSGAF	LiCAF
λ_p (nm)	653	653	653
λ_c (nm)	850	830	780
n	1.41	1.41	1.41
τ_r (μs)	67	88	190
τ_{nro} (10^{-14}s)	2.4	6.9	1.3
ΔE (cm^{-1})	5125	5155	8532
α_p (cm^{-1})	6.81	6.81	6.81
k (W/°Kcm)	0.031	0.035	0.485
γ ($10^{16}cm^3/s$)	6.5	6.5	1.65

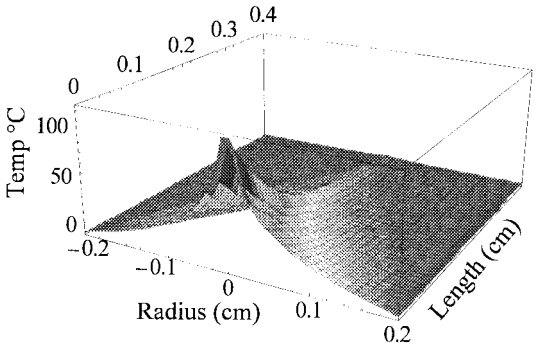

Fig. 3. Temperature rise in a 1.5% Cr:LiSAF laser rod as a function of radius and length in the laser rod for 1000 mW of incident pump power.

The total amount of pump power converted into heat in the crystal is found by integrating the total thermal power density over the crystal volume

$$P_{\rm th} = \int_{z=0}^{l} \int_{r=0}^{b} \frac{dP_{\rm th}}{dV} 2\pi r \; dr \; dz. \tag{16}$$

The percentage of pump power converted into heat (ε) is found by dividing the total thermal power $(P_{\rm th})$ by pump power incident on the crystal $(P_{\rm po})$.

III. MODEL ESTIMATES OF THE TEMPERATURE DISTRIBUTION

The equations deduced in the previous section have been used to estimate the temperature distribution inside different colquiriite laser rods for several values of the pump power. The solution to the heat equations assumes that the thermal power density has a Gaussian radial distribution and an exponential decay in the z direction. The temperature distribution inside the crystal is determined using a recursive method similar to that described by Balembois *et al.* [14].

First, the equation for the thermal power density is solved using only the quantum defect heating effect. This is done because quantum defect heating is not temperature-dependent. The amount of pump power converted into heat is then calculated by the method discussed above. The first spatial temperature distribution is calculated, with the results inserted into the temperature-dependent lifetime formula (13) to determine the spatial profile of the upper state lifetime. This new upper state lifetime profile changes the upper state population density profile, which changes both the upconversion and the thermal quenching of fluorescence thermal power density.

The thermal power density, now including the heating sources due to quantum defect, upconversion, and thermal quenching of fluorescence, is integrated over the volume of the crystal to determine the total thermal power and the percentage of the pump power converted into heat (ε).

Since the model requires that the total thermal power density has an exponential decay in the z direction, the newly calculated thermal power density is fitted to an exponential decay. This fit determines the power density absorption coefficient $\alpha_{\rm therm}$. These new data (ε and $\alpha_{\rm therm}$) are then inserted back into (3) to recalculate a new temperature distribution. The whole process is then repeated with the temperature and upper state population converging to a stable solution after five iterations.

Described below are model calculations for the resulting temperature distributions for different values of the pump power $P_{\rm po}$. These calculations are then repeated for several different colquiriite crystal materials. These estimates are made for realistic pump beam dimensions within rods of sizes commonly used for diode pumped colquiriites. In addition, the effect the temperature rise has on the upper state lifetime is calculated. The model assumes there is no stimulated emission, no laser resonator around the rod, and therefore no extracted optical laser power from the rod. The calculations also show the relative contributions to the thermal power density coming from the heating effects of quantum defect, upconversion, and thermal quenching of fluorescence. Without a resonator around the laser rod, the calculated results which follow are a conservative upper estimate of the magnitude of the heating effects inside the laser rod.

A. Cr:LiSAF

The temperature increase above room temperature in a 4-mm-diameter×4-mm-long, 1.5% Cr:LiSAF laser rod for 1 W of pump power is shown in Fig. 3. The Gaussian pump beam has a 38 micron diameter at the input face of the crystal. The pump wavelength entered into the code is 653 nm which is the weighted average for the 647 and 676 Krypton ion laser lines. The center fluorescence wavelength is set to 850 nm at the peak of the LiSAF emission cross section. The thermomechanical parameters entered into the code are shown in Table I. For 1 W of pump power, Fig. 3 shows that the induced temperature gradient (ΔT) inside the laser crystal is over 100 °C.

Fig. 4(a) and (b) shows the upper-state lifetime as function of radius and depth in the crystal for 500 mW and 1 W of pump power, respectively. At a pump power of 500 mW, there is a small dip in lifetime at the center of the front face of the LiSAF crystal. This dip is caused by the small volume near the front face where the temperature has exceeded the critical temperature. When the pump power is increased to 1 W of power, the temperature rise at the input face of the crystal is so large that the upper state lifetime has fallen to zero in that region, as shown in Fig. 4(b). The impact that this upper state lifetime decrease has on the upper state population density can

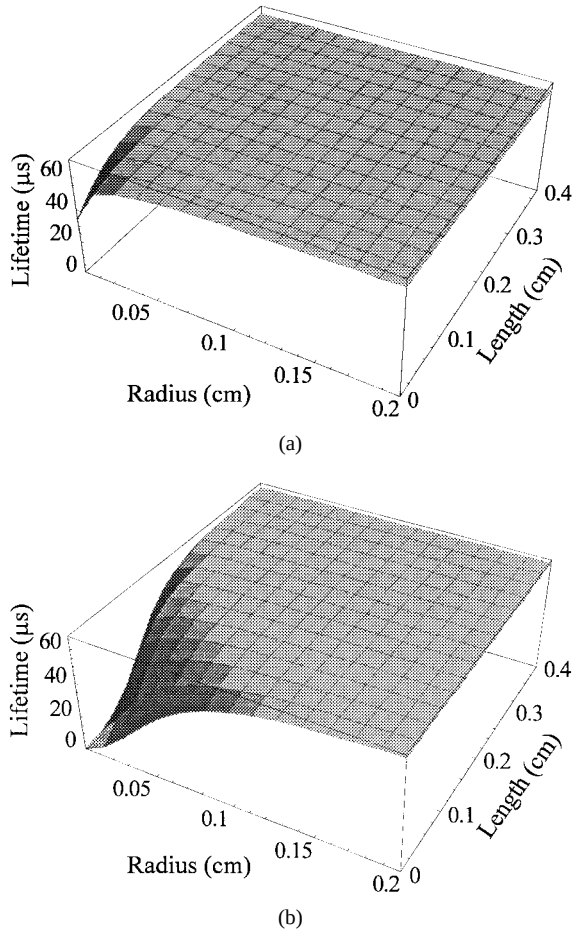

Fig. 4. Upper state lifetime distribution as a function of radius and length in the laser rod for (a) 500 mW and (b) 1000 mW of incident pump power.

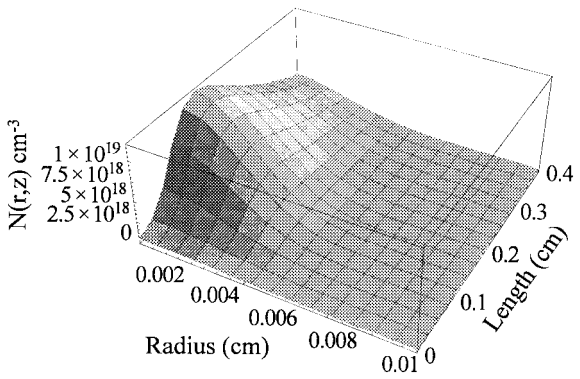

Fig. 5. Upper state population density distribution $N(r, z)$ as a function of radius and length in the laser rod for 1000 mW of incident pump power.

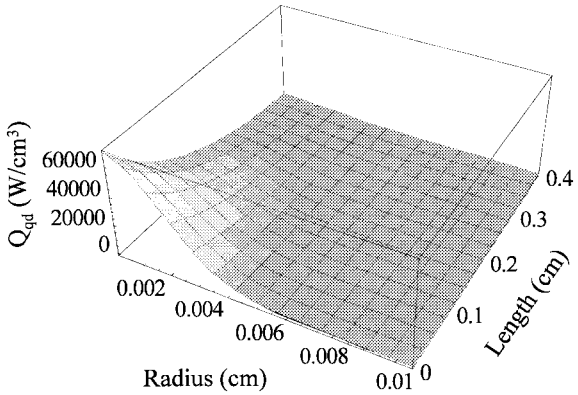

Fig. 6. Quantum defect heating power density as a function of radius and length in the laser rod for 1000 mW of incident pump power.

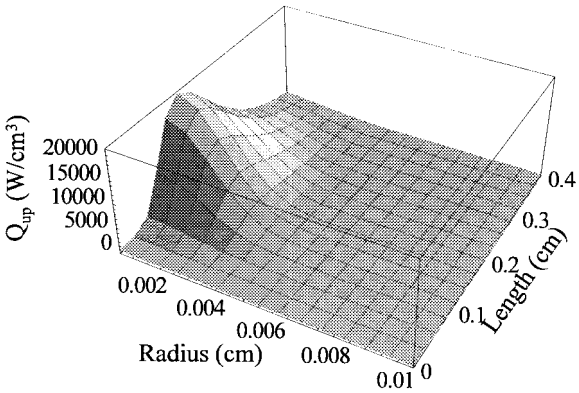

Fig. 7. Upconversion heating power density as a function of radius and length in the laser rod for 1000 mW of incident pump power.

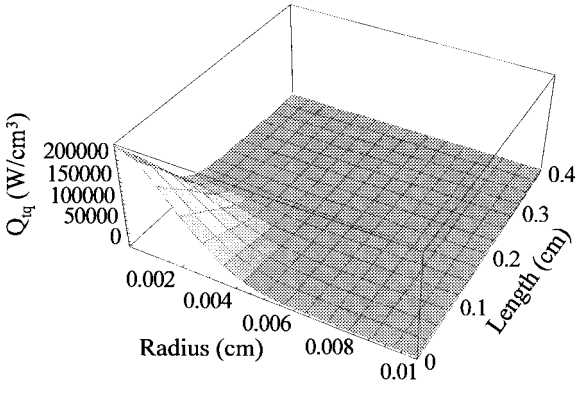

Fig. 8. Thermal quenching of fluorescence heating power density as a function of radius and length in the laser rod for 1000 mW of incident pump power.

be seen in Fig. 5. When the pump power is at this high level, the upper state population can be severely depleted. This is important to note because the upper state population is zero despite the fact that the pumping density is the highest at the front face of the crystal. The upper state population depletion leads to a decrease in gain with increased pump power.

Figs. 6–8 illustrate the relative magnitude and location of the quantum defect, upconversion, and thermal quenching heating sources in the LiSAF crystal for 1 W of pump power.

It can be seen that the quantum defect has a large effect on the center axis of the rod where the pumping density is highest. The quantum defect heating spatial distribution is identical to the pump beam spatial distribution which agrees with (7) in the theory. At high pump powers (1 W), there is little heating from upconversion at the center of the beam (Fig. 7) because of the aforementioned depletion of upper state population at the front face of the rod. As shown in (10), the upconversion heating is proportional to the square of the upper state population density.

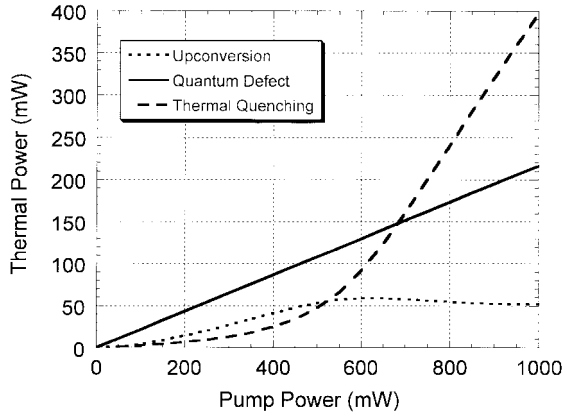

Fig. 9. Plot of quantum defect, upconversion, and thermal quenching power deposited in a 1.5% Cr:LiSAF laser rod for pump power ranging from 0 to 1000 mW.

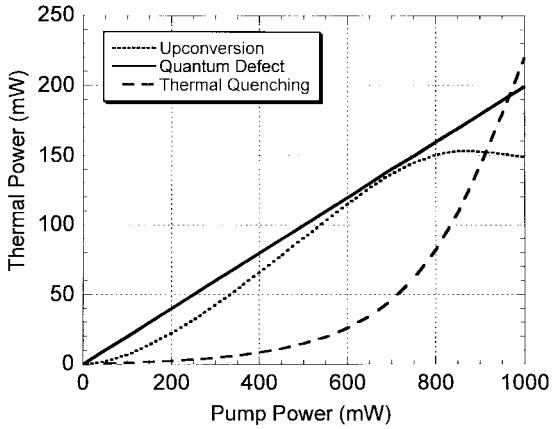

Fig. 10. Plot of quantum defect, upconversion, and thermal quenching power deposited in a 1.5% Cr:LiSGAF laser rod for pump power ranging from 0 to 1000 mW.

The code correctly shows that the reduction in upper state population near the front face eliminates the opportunity for upconversion heating to occur. Therefore, as the pump power is increased, upconversion heating slowly decreases.

As can be seen in Fig. 8, the thermal quenching of fluorescence is greatest at the center of the front face of the crystal. The spatial distribution of thermal quenching of fluorescence heating changes little with pump power. However, the peak value of the thermal quenching power density at the center of the rod for 1 W of power is five times higher than the peak value of the power density for 500 mW of pump.

As described in (16), the total thermal power which is deposited in the crystal is calculated by integrating the total thermal power density over the volume of the crystal. The thermal power due to each individual heating source can be found by integrating each thermal power density individually. The thermal powers for each source are shown in Fig. 9 for pump powers ranging from 0 to 1 W.

At low pump powers, ($<$400 mW), the quantum defect is the predominant heating source. The upper state population density is increasing and likewise upconversion heating is increasing. Thermal quenching of fluorescence is insignificant at these power levels because the temperature of the rod is still well below the critical temperature for nonradiative decay. For 400 mW of pump power, approximately one-third of the pump power is converted into heat.

At moderate power levels (400–700 mW), there is a considerable change inside the laser rod. As the pump power is increased above 400 mW, the temperature begins to rise inside the rod and thermal quenching increases significantly. Upconversion heating also increases until approximately 600 mW of pump power where it peaks and then begins to slowly decrease because the upper state population density is slowly decreasing due to upper state lifetime quenching. By doubling the pump power from 500 mW to 1 W, the upper state population density is nearly constant. For these pump conditions, any increase in pump power above 1 W is wasted as heat inside the crystal. Fig. 9 shows graphically that as the pump power increases above 600 mW a type of thermal runaway occurs. This happens when the rod temperature approaches the critical temperature for nonradiative decay. Over one-half of the pump power is directed into crystal heating for 650 mW of pump power.

At higher pump powers ($>$700 mW), thermal quenching of fluorescence is the largest heating source. With the temperature at the center of the rod well above the critical temperature for nonradiative decay, upconversion heating is decreasing due to the depleted upper state population. For 1 W of pump power, approximately two-thirds of the pump power is directed into crystal heating.

It should be noted that our model, while similar to that described in [14], assumes a larger pump spot size and a shorter pump wavelength. These differences result in greater quantum defect heating and a higher pump power at which the thermal runaway occurs.

B. LiSGAF

We recalculated the temperature increase above room temperature for a 4-mm-diameter $\times$ 4-mm-long, 1.5% Cr:LiSGAF laser rod for pump powers ranging from 0 to 1 W. The pump conditions were identical to those described above. The center fluorescence wavelength was 830 nm, at the peak of the LiSGAF emission cross section. The thermomechanical parameters used in the code are shown in Table I. The induced temperature gradient (ΔT) inside the laser crystal is approximately 80 °C for the same pump conditions as in the LiSAF results. This temperature rise is over 20 °C less than for LiSAF with the exact same pump conditions and dopant concentration.

The thermal powers deposited inside the LiSGAF crystal for quantum defect, upconversion, and thermal quenching heating are shown in Fig. 10 for pump powers ranging from 0 to 1 W. For power levels up to 800 mW, both upconversion and quantum defect play a similar role in heating up the laser crystal. Thermal quenching does not become a significant heating source until the pump power reaches $\sim$700 mW. Thermal quenching of fluorescence is insignificant up to this high pump power because the critical temperature for nonradiative decay in LiSGAF is 88 °C. A thermal runaway rapidly occurs in LiSGAF above 900 mW of pump power.

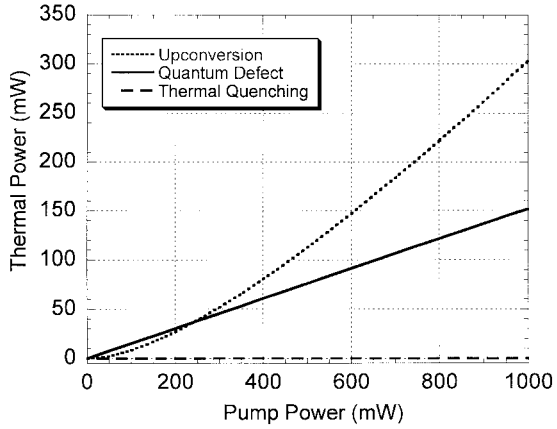

Fig. 11. Plot of quantum defect, upconversion, and thermal quenching power deposited in a 1.5% Cr:LiCAF laser rod for pump power ranging from 0 to 1000 mW.

At this point, thermal quenching of fluorescence is the major heating source. Upconversion heating begins to decrease at these high power levels because of the thermally induced upper state population decrease.

C. LiCAF

We recalculated the temperature increase inside a 4-mm-diameter × 4-mm-long, 5% Cr:LiCAF laser rod as a function of input pump powers ranging from 0 to 1 W. The pump conditions are identical to those described above for LiSAF and LiSGAF. The center fluorescence wavelength is set to 780 nm, the peak of the LiCAF emission cross section. The thermomechanical parameters entered into the code for LiCAF are shown in Table I. The induced temperature gradient (ΔT) inside the laser crystal is only 40 °C. This is over 60 °C cooler than LiSAF and 40 °C cooler than LiSGAF with the same pump conditions and pump wavelength absorption coefficient. The absorption coefficient for 5% Cr:LiCAF is approximately the same as 1.5% Cr:LiSAF and 1.5% Cr:LiSGAF.

The thermal powers density for quantum defect, upconversion, and thermal quenching of fluorescence are shown in Fig. 11 for pump powers ranging from 0 to 1 W. There is no thermal quenching of fluorescence at these power levels in LiCAF because of the high critical temperature for nonradiative decay in LiCAF (190 °C). As seen from Fig. 11, quantum defect heating in LiCAF is also low when compared to LiSAF and LiSGAF because the pump wavelength (653 nm) is much closer to the center fluorescence wavelength (780 nm). The lack of thermal quenching and the low quantum defect lead to a rapid buildup of the upper state population. This has the unfortunate result of producing a large amount of upconversion heating. This is despite the fact that LiCAF has four times less upconversion than LiSAF [16], [17], [19], [20]. Thus, the limiting factor in any LiCAF laser rod is upconversion, not thermal quenching of fluorescence as it is in LiSAF and LiSGAF.

IV. Thermal Lensing

The pump-induced temperature gradient across the laser rod creates stresses inside the laser medium. As the laser media heats up, the material expands and contracts. These movements cause internal stresses to build up within the laser rod. These stresses can cause the index of refraction to change in a localized area of the rod. These stress-induced index of refraction changes combined with the temperature-dependent index of refraction can induce severe optical distortions to a laser beam passing through the laser media [38]. One of the optical distortions caused by these stresses is thermal lensing.

TABLE II
Thermal Properties of Colquiriites

Property	LiSAF	LiSGAF	LiCAF
dn/dt (10^{-6}/ °C) ∥c	-4.0	-	-4.6
dn/dt (10^{-6}/ °C) ⊥c	-2.5	-	-4.2
α (10^{-6}/ °C) ∥c	-10	0	3.6
α (10^{-6}/ °C) ⊥c	25	12	22

To quantify the effect of thermal lensing on a laser media, the lensing power of an isotropic material can be described by [22], [38], [39]

$$f_{r,\phi}^{-1} = \frac{4l\Delta T}{r^2}\left[\frac{1}{2}\frac{dn}{dT} + \alpha C_{r,\phi} n^3 + \frac{\alpha r(n-1)}{l}\right] \qquad (17)$$

where n is refractive index, dn/dT is the change of refractive index with temperature ($1/°\mathrm{C}$), α is the coefficient of thermal expansion ($°\mathrm{C}^{-1}$), ΔT is the temperature difference between the center of the rod and the edge of the rod, r is the radius of the rod, and l is the length of the rod. The first term in (17), dn/dT, describes the refractive index change induced by the change in temperature. The second term $C_{r,\phi}$ is the linear combination of photoelastic constants that result from temperature-induced stress inside the crystal. The last term describes the physical distortions to the ends of the rod, causing it to act as a lens.

A summary of these measured thermomechanical properties for the colquiriites is shown in Table II. The temperature-dependent refractive index (dn/dT) in LiCAF and LiSAF have been quantitatively measured to be negative [22], [25]. The negative thermal refractive coefficient is typical of the fluoride laser crystals [39]. If dn/dT was the only contribution to thermal lensing, the colquiriites would exhibit negative thermal lensing. However, since the stress-optic coefficient $(C_{r,\phi})$ is nearly always positive [39], the linear combination of the temperature- and stress-induced refractive index changes tend to cancel, resulting in reduced positive thermal lensing. In contrast, in oxide laser crystals such as Nd:YAG, the temperature- and stress-induced refractive index changes are additive, resulting in stronger thermal lensing. More quantitative results in our lensing theory is hindered by the fact that the $C_{r,\phi}$ terms have not yet been measured in any of the colquiriite crystals. In one work, the values for the $C_{r,\phi}$ terms in LiCAF were approximated by using the values for CaF_2 [22].

V. Experimental Measurement of Thermal Lensing

The inability to accurately calculate the amount of thermally induced lensing forced us to make experimental measurements of the parameter in each colquiriite laser host. The theoretical calculations were made in order to determine the physical limits to scaling the colquiriites to higher average powers. The

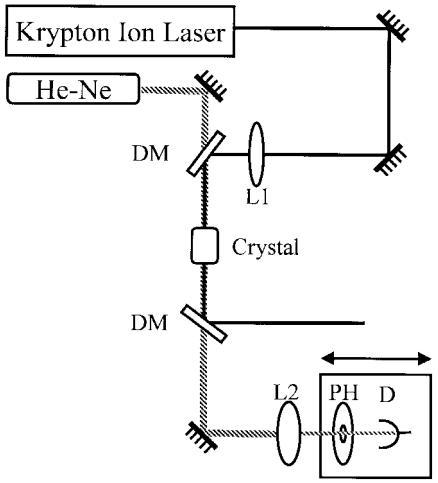

Fig. 12. Experimental setup for thermal lensing measurements. $L1 = 10$ cm PL/CX lens, DM: dichroic mirror, HR 650 nm, HT 543 nm, $L2 = 15$ cm PL/CX lens, $\mathrm{PH} = 50$ μm pinhole, $D =$ Detector.

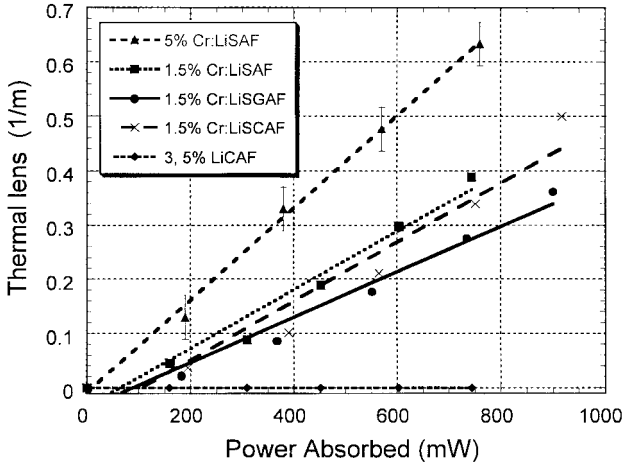

Fig. 13. Experimental data showing thermal lensing focal power versus absorbed pump power.

results of these thermal lensing experiments are being used to assist in the development a high-average-power diode-pumped tunable colquiriite laser system.

The optical layout for the experimental measurement of thermally induced lensing is shown in Fig. 12. Diode pumping in these experiments was simulated with the use of a high-quality krypton ion laser. The pump laser (Spectra-Physics 2017) was operated on both the 647- and 676-nm red lines (power ratio 4:1) in a single transverse mode and was linearly polarized. The use of a krypton ion laser simplifies the calculation of the thermal lens because of its Gaussian mode profile. The induced thermal lensing was monitored with a CW probe laser. The probe laser was a linearly polarized green (543.5 nm) helium neon laser. The probe laser was collimated and passed through the center of the colquiriite crystal. Collimation of the probe laser was verified using a lateral shearing interferometer. The two lasers were combined with a dichroic mirror and aligned to overlap spatially inside the laser crystal. The polarization of both lasers were adjusted such that their electric fields were parallel to the crystalline c axis. The krypton-ion pump beam was focused into the crystal with a 10-cm focal length plano–convex lens resulting in a calculated 38-μm pump radius inside the crystal. After passing through the laser crystal, a dichroic mirror separated the two beams and the system alignment was verified by analyzing the probe beam spatial profile with a two-dimensional (2-D) CCD array (Spiricon LBA-100A). An increase in pump power only resulted in a change to the probe beam diameter and did not induce any ellipticity or pointing drift onto the probe beam.

To measure the effective focal length of the laser crystals, the technique discussed by Burnham [40] was used. This technique is very sensitive to small changes in the probe beam divergence. The probe beam was focused with a 15-cm plano-convex lens through a 50-μm-diameter pinhole. A calibrated power meter (Coherent Labmaster with LM-2 detector head) detected the transmitted power through the pinhole. The laser crystals were pumped with the krypton-ion laser for one half hour to ensure that the crystals were in thermal equilibrium with the temperature controlled laboratory environment. The beam waist of the focused probe beam was determined by scanning the position of the pinhole along the z axis. In order to effectively remove heat from the laser samples, each sample was lined with a 0.005-in-thick layer of indium foil before being placed into the heat sink. The indium was used because of its excellent thermal conductivity and the indium foil allows the laser crystals to expand without placing additional strain onto the crystal lattice.

The thermally induced focal length is calculated using the general equation for a two-component system [41]

$$f_{\mathrm{th}} = d - f + \frac{f^2}{\Delta S} \tag{18}$$

where d is the distance between the crystal and the probe beam focusing lens (m), f is the focal length of the probe beam focusing lens (m), and ΔS is the displacement of the beam waist due to the thermal lens (m).

The measured thermally induced focal power $(1/f_{\mathrm{th}})$ of the colquiriite laser samples are shown in Fig. 13. The figure shows the induced focal power for 1.5% and 5% Cr:LiSAF, 1.5% Cr:LiSGAF, 3% Cr:LiSCAF, and 3% and 5% Cr:LiCAF plotted as a function of absorbed pump power. The data shown in Fig. 13 shows that the thermal focal length is nearly inversely proportional to the absorbed pump power, in good agreement with thermal lensing theory [4]. It should be noted that we were unable to measure any thermally induced lensing in Cr:LiCAF in this experimental setup. The strongest thermally induced focal length in these experiments was over 1.5 m long.

VI. Discussion

As noted earlier in Section IV, if the thermal lensing in the laser rods were only the result of the temperature-induced index gradient, the sign of the thermal lens should be negative.

However, as the pump power was increased, we measured weak positive thermal lensing. We believe this low amount $(f_{\mathrm{th}} > 1$ m) of positive, thermally induced lensing in these colquiriite materials is a direct result of the compensation of

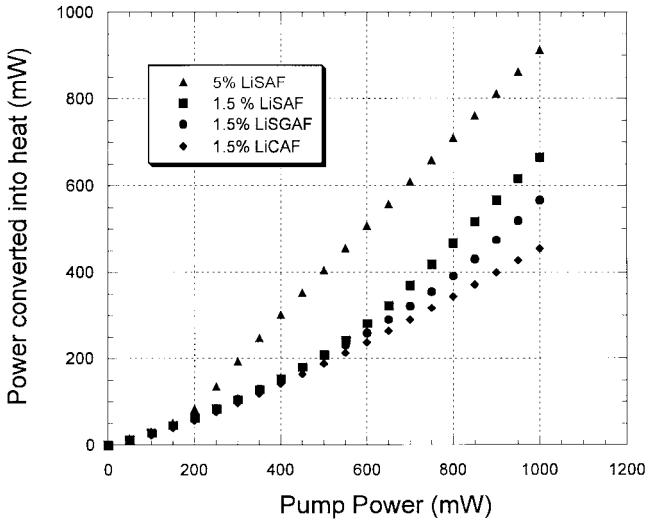

Fig. 14. Plot of heating in the colquiriites for pump power ranging from 0 to 1000 mW.

negative dn/dT by the positive stresses and expansion of the crystal.

We were unable to measure any thermal lensing in two different LiCAF samples with pump powers of over 1 W. However, weak thermal lensing behavior has been observed in a flashlamp-pumped LiCAF system [22], [38]. From the latter, approximate values for $C_{r,\phi}$ were then used to help theoretically explain why the LiCAF had less thermally induced lensing than alexandrite [22].

We believe the different thermal lensing signals for each material are the direct result of two different contributing factors.

First, each material has slightly different thermomechanical properties, specifically the critical temperature for quenching of fluorescence. Therefore, for identical pump conditions, each colquiriite material converts a different amount of the pump power to heat, resulting in different temperature gradients across the laser rod. Fig. 14 shows the total amount of pump power converted into heat as a function of the pump power for LiSAF, LiSGAF, and LiCAF. LiSCAF's thermomechanical properties, to our knowledge, have never been measured. As expected, the highly doped 5% LiSAF heats more than the 1.5% LiSAF, due to the higher absorption coefficient. As discussed above, the LiSGAF heats less than the LiSAF since the critical temperature is lower in LiSAF than in LiSGAF. LiCAF heats the least of all the colquiriite materials because of the low amount of thermal quenching of fluorescence.

Second, the differences in thermal lensing can also be explained by the fact that each material has slightly different numerical values for dn/dT and $C_{r,\phi}$. As shown in (17) for identical temperature gradients, these differences can change the power of the thermal lens. The reduced thermal lensing in LiCAF by Woods *et al.* [22] was explained by concluding that the compensation of the negative dn/dT by the positive stress $C_{r,\phi}$ resulted in reduced thermal lensing. If dn/dT and $C_{r,\phi}$ are not extremely close, as in the case of LiCAF, then, given the high temperature gradients inside these materials, the thermal lensing can quickly become quite strong.

VII. Conclusion

We have measured the pump-induced thermal lensing of Cr^{3+}-doped colquiriites in a sensitive experimental setup. To assist in the development of high-average-power diode-pumped tunable laser systems, we have also developed a new computer model that calculates the temperature rise inside any colquiriite laser crystal. These measurements are critical to the proper choice and design of high-power diode-pumped colquiriite lasers. The thermal code is essential to determining the correct material and dopant level required. We have utilized the output of this code to help explain the differences in measured thermal lensing power in the colquiriite materials.

The colquiriites are attractive because of the small amount of thermal lensing when compared to other solid-state materials such as Nd:YAG and alexandrite. The strongest thermally induced lens measured in our experiments was over 1.5 m long. The reduced lensing in LiCAF combined with its superior temperature-dependent lifetime and thermomechanical properties make it a promising colquiriite material. However, the poor optical quality and large amount of scattering in currently available LiCAF limits the potential of this material at this time. We have also shown that the laser material, LiSGAF, is a compromise between the superior thermomechanical and thermal lensing properties of LiCAF and the less favorable thermomechanical and thermal lensing properties of LiSAF. With improvements to its optical quality and scattering, LiCAF could become the clear choice for a high-average-power tunable laser-diode-pumped laser system.

Acknowledgment

The authors thank B. H. T. Chai, H. P. Jenssen, and A. Casannho for growing the laser crystals used in these studies. They also thank M. Yamanaka and M. Bass for the many useful discussions about this work, J. Cormier for machining the crystal heatsinks, and M. Silver for assistance in polishing the LiCAF and LiSCAF samples.

References

[1] A. K. Cousins, "Temperature and thermal stress scaling in finite-length end-pumped laser rods," *IEEE J. Quantum Electron.*, vol. 28, pp. 1057–1069, 1992.
[2] T. Y. Fan and A. Sanchez, "Pump source requirements for end-pumped lasers," *IEEE J. Quantum Electron.*, vol. 26, pp. 311–316, 1990.
[3] M. Ohmi, K. Naito, K. Ishikawa, M. Akatsuku, T. Sato, M. Yamanaka, and S. Nakai, "Parametric studies on the laser-diode-pumped, thermal-lensing-compensated mode-locked, Q-switched Nd:YAG laser," *Jpn. J. Appl. Phys.*, vol. 33, no. 5A, pp. 2579–2585 1994.
[4] W. Koechner, *Solid State Laser Engineering*, 4th ed. New York: Springer-Verlag, 1996.
[5] D. F. Welch and D. R. Scifres, "High power, 8.5 W CW, visible laser diodes," *Electron. Lett.*, vol. 27, no. 21, pp. 1915–1916, 1991.
[6] H. B. Serreze, C. M. Harding, and R. G. Waters, "1 W CW, 672 nm visible laser diodes," *Electron. Lett.*, vol. 27, no. 24, pp. 2245–2246, 1991.
[7] J. M. Hayden, D. W. Nam, D. F. Welch, J. G. Endriz, and D. R. Scifres, "High power 60 W quasi-CW, visible laser diode arrays," *Electron. Lett.*, vol. 28, no. 5, pp. 451–452, 1992.
[8] H. Jaeckel, G. L. Bona, H. Richard, P. Roentgen, and P. Unger, "Reliable 1.2 W CW red-emitting (Al)GaInP diode laser array with AlGaAs cladding layers," *Electron. Lett.*, vol. 29, no. 1, pp. 101–102, 1993.
[9] J. A. Skidmore, M. A. Emanuel, R. J. Beach, W. J. Benett, B. L. Freitas, N. W. Carlson, and R. W. Solarz, "High-power continuous wave 690 nm

AlGaInP laser diodes," *Appl. Phys. Lett.*, vol. 66, no. 2, pp. 1163–1165, 1995.
[10] D. Kopf, U. Keller, M. A. Emanuel, R. J. Beach, and J. A. Skidmore, "1.1-W cw Cr:LiSAF laser pumped by a 1-cm diode array," *Opt. Lett.*, vol. 22, no. 2, pp. 99–101, 1997.
[11] P. Beaud, Y.-F. Chen, B. H. T. Chai, and M. C. Richardson, "Gain properties of $LiSrAlF_6$:Cr^{3+}," *Opt. Lett.*, vol. 17, No. 15, pp. 1064–1066, 1992.
[12] F. Balembois, F. Druon, F. Falcoz, P. Georges, and A. Brun, "Performances of Cr:$LiSrAlF_6$ and Cr:$LiSrGaF_6$ for continuous-wave diode-pumped Q-switched operation," *Opt. Lett.*, vol. 22, no. 6, pp. 387–389, 1997.
[13] F. Hanson, C. Bendall, and P. Poirier, "Gain measurements and average power capabilities of Cr^{3+}:$LiSrAlF_6$," *Opt. Lett.*, vol. 18, No. 17, pp. 1423–1425.
[14] F. Balembois, F. Falcoz, F. Kerboull, F. Druon, P. Georges, and A. Brun, "Theoretical and experimental investigation of small-signal gain for a diode pumped Q-switched Cr:LiSAF laser," *IEEE J. Quantum Electron.*, vol. 33, pp. 269–277, 1997.
[15] L. K. Smith, S. A. Payne, W. L. Kway, L. L. Chase, and B. H. T. Chai, "Investigation of the laser properties of Cr^{3+}:$LiSrGaF_6$," *IEEE J. Quantum Electron.*, vol. 28, pp. 2612–2618, 1992.
[16] W. R. Rapoport, "Excited-state absorption and upconversion in Cr:LiSAF," in *OSA Proc. Advanced Solid State Lasers*, L. L. Chase and A. A. Pinto, Eds., Washington, DC, 1992, pp. 21–27.
[17] P. Beaud, M. C. Richardson, Y.-F. Chen, and B. H. T. Chai, "Optical amplification characteristics of Cr:LiSAF and Cr:LiCAF under flashlamp pumping," *IEEE J. Quantum Electron.*, vol. 30, pp. 1259–1266, 1994.
[18] H. W. Lee, S. A. Payne, and L. L. Chase, "Excited-state absorption of Cr^{3+} in $LiCaAlF_6$: Effects of asymmetric distortions and intensity selection rules," *Phys. Rev. B*, vol. 39, no. 13, pp. 8907–8914, 1989.
[19] M. A. Noginov, H. P. Jenssen, and A. Cassanho, "Upconversion in Cr:LiSGAF and Cr:LiSAF," in *OSA Proc. Advanced Solid State Lasers*, A. A. Pinto and T. Y. Fan, Eds., Washington, DC, 1993, pp. 376–380.
[20] M. A. Noginov, V. G. Ostroumov, I. A. Shcherbakov, V. A. Smirnov, and D. A. Zubenko, "Interaction of excited Cr^{3+} ions in laser crystals," in *OSA Proc. Advanced Solid State Lasers*, G. Dube and L. L. Chase, Eds., Washington, DC, 1991, pp. 21–24.
[21] S. A. Payne, L. K. Smith, R. J. Beach, B. H. T. Chai, J. H. Tassano, L. D. DeLoach, W. L. Kway, R. W. Solarz, and W. F. Krupke, "Properties of Cr:$LiSAF_6$ crystals for laser operation," *Appl. Opt.*, vol. 33, no. 24, pp. 5526–5536, 1994.
[22] B. W. Woods, S. A. Payne, J. E. Marion, R. S. Hughes, and L. E. Davis, "Thermo-mechanical and thermo-optical properties of the $LiCaAlF_6$:Cr^{3+} laser material," *J. Opt. Soc. Amer. B*, vol. 8, no. 5, pp. 970–977, 1991.
[23] M. Richardson, M. J. Soileau, P. Beaud, R. De Salvo, S. Garnov, D. J. Hagan, S. Klimentov, K. Richardson, M. Sheik-Bahae, A. A. Said, E. Van Stryland, and B. H. T. Chai, "Self focusing and optical damage in Cr:LiSAF and Cr:LiCAF," in *1992 Proc. SPIE Laser-Induced Damage in Optical Materials*, vol. 1848, pp. 392–402.
[24] M. Stadler, M. Bass, and B. H. T. Chai, "Thermal quenching of fluorescence in chromium-doped fluoride laser crystals," *J. Opt. Soc. Amer. B*, vol. 9, no. 12, pp. 2271–2273, 1992.
[25] S. A. Payne, W. F. Krupke, L. K. Smith, W. L. Kway, L. D. DeLoach, and J. B. Tassano, "752 nm wing-pumped Cr:LiSAF laser," *IEEE J. Quantum Electron.*, vol. 28, pp. 1188–1196, 1992.
[26] Y. Jin, M. Hongxiang, and J. Tianfeng, "Modeling of thermal lensing in CW end-pumped solid state lasers," *SPIE*, vol. 2889, pp. 171–177, 1996.
[27] J. P. Gordon, R. C. C. Leite, R. S. Moore, S. P. S. Porto, and J. R. Whinnery, "Long-transient effects in lasers with inserted liquid samples," *J. Appl. Phys.*, vol. 36, no. 1, pp. 3–8, 1965.
[28] W. Koechner, "Thermal lensing in a Nd:YAG laser rod," *Appl. Opt.*, vol. 9, no. 11, pp. 2548–2553, 1970.
[29] B. Neuenschwander, R. Weber, and H. P. Weber, "Thermal lens and beam properties in multiple longitudinally diode laser pumped Nd:YAG slab lasers," *IEEE, J. Quantum Electron.*, vol. 32, pp. 365–370, 1996.
[30] G. Cerullo, S. De Silvestri, and V. Magni, "Self-starting Kerr-lens mode locking of a Ti:sapphire laser," *Opt. Lett.*, vol. 19, no. 14, pp. 1040–1042, 1994.
[31] A. Ritsataki, G. H. C. New, R. Mellish, J. Plumridge, P. M. W. French, and J. R. Taylor, "Experimental and theoretical investigations of all-solid-state Kerr lens mode-locked lasers," in *OSA Proc. Advanced Solid State Lasers*, Washington, DC, 1997, p. 143, paper MF7.
[32] M. E. Innocenzi, H. T. Yura, C. L. Fincher, and R. A. Fields, "Thermal modeling of continuous-wave end-pumped solid-state lasers," *Appl. Phys. Lett.*, vol. 56, no. 19, pp. 1831–1833, 1990.
[33] D. Kopf, J. Aus der Au, U. Keller, G. L. Bona, and P. Roentgen, "400-mW continuous-wave diode-pumped Cr:LiSAF laser based on a power-scalable concept," *Opt. Lett.*, vol. 20, no. 17, pp. 1782–1784, 1995.
[34] U. O. Farrukh, A. M. Buoncristiani, and C. E. Byvik, "An analysis of the temperature distribution in finite solid-state laser rods," *IEEE J. Quantum. Electron.*, vol. 24, pp. 2253–2263, 1988.
[35] R. A. Fields, T. S. Rose, M. E. Innocenzi, H. T. Yura, and C. L. Fincher, "Diode laser end-pumped neodymium lasers: The road to higher powers," in *OSA Proc. Tunable Solid State Lasers*, 1989, p. 301.
[36] H. S. Carslaw, *Conduction of Heat in Solids*. Oxford, U.K.: Clarendon, p. 1959, 191.
[37] M. Abramawitz and I. A. Stegun, Eds., *Handbook of Mathematical Functions*. New York: Dover, 1970, p. 228.
[38] J. S. Uppal and J. Monga, "Contribution of stress-dependent variation of refractive index to thermal lensing in Nd:glass laser rods," *Appl. Opt.*, vol. 24, no. 22, pp. 3690–3692, 1985.
[39] L. L. Chase, S. A. Payne, R. S. Hughes, B. W. Woods, and L. E. Davis, "Measurement of thermal lensing for the $LiCaAlF_6$:Cr^{3+} laser material," in *OSA Proc. Tunable Solid State Lasers*, 1990, pp. 83–85.
[40] D. C. Burnham, "Simple measurement of thermal lensing effects in laser rods," *Appl. Opt.*, vol. 9, no. 7, pp. 1727–1728, 1970.
[41] W. J. Smith, *Modern Optical Engineering*, 2nd ed. New York: McGraw-Hill, 1990, p. 45.

Jason M. Eichenholz received the B.S. degree in physics from Rensselaer Polytechnic Institute, Troy, NY, in 1992 and the M.S. degree in optical sciences and engineering from the University of Central Florida, Orlando, in 1995. He is currently working towards the Ph.D. degree at the same insitution. His dissertation focuses on high-power diode pumping of the colquiriites.

His research interests are in the area of diode pumping of new solid-state laser materials.

Mr. Eichenholz is a student member of the Optical Society of America and SPIE.

Martin Richardson received the Ph.D. degree from London University, U.K.

He is currently Professor of Physics and Electrical and Computer Engineering at the University of Central Florida, Orlando. His current interest focuses on applications of point source laser plasmas—X-rays—particularly in lithography and kinetic effects in materials, the development of new high-power solid-state lasers and their applications, the advancement of high time and spatial resolution X-ray optical and electrooptical instrumentation, the development of X-ray microscopy for the biological medical sciences, and the development of ultrashort, high-intensity lasers for X-ray generation, dense plasma physics, and high field of physics.

Dr. Richardson is a fellow of the Optical Society of America.